LANGMUIR

pubs.acs.org/Langmuir Article

Grafting To of Bottlebrush Polymers: Conformation and Kinetics

Luis A. Navarro, Tejank P. Shah, and Stefan Zauscher*



Cite This: Langmuir 2020, 36, 4745-4756



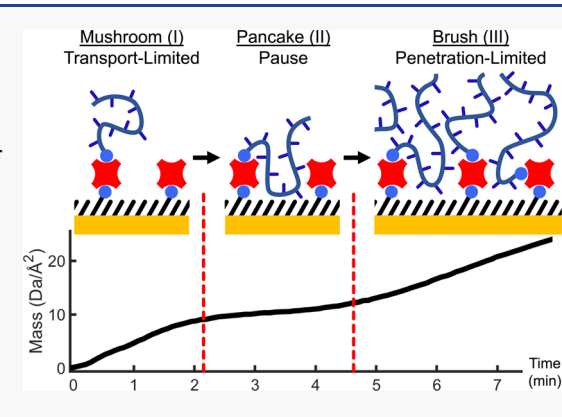
ACCESS

III Metrics & More

Article Recommendations

Supporting Information

ABSTRACT: Specifically adsorbed bottlebrush coatings are found in nature as brush-like glycoproteins that decorate biointerfaces and provide antifouling, lubrication, or wear-protection. Although various synthetic strategies have been developed to mimic glycoprotein structure and function, the use of these mimics is still limited because of the current lack of understanding of their adsorption behavior and surface conformation. In this paper, we examine the adsorption behavior of PEG-based, biotinylated bottlebrushes with different backbone and bristle lengths to streptavidin model surfaces in phosphate-buffered saline. By using quartz crystal microbalance, localized surface plasmon resonance, and atomic force microscopy, we learn how bottlebrush dimensions impact their adsorption kinetics, surface conformation, mechanical properties, and antifouling properties. Our bottlebrushes qualitatively mirror the adsorption behavior of linear polymers and exhibit three kinetic regimes of adsorption: (I) a



transport-limited regime, (II) a pause, and (III) a penetration-limited regime. Furthermore, we find that the bristle length more dramatically affects brush properties than the backbone length. Generally, larger bottlebrush dimensions lead to reduced molar adsorption, retarded kinetics, weaker antifouling, and softer brush coatings. Longer bristles also lead to less mass adsorption, while the opposite trend is observed for increasing backbone length. In summary, our findings aid the rational design of new bottlebrush coatings by elucidating how their dimensions impact adsorption, surface conformation, and the properties of the final coating.

INTRODUCTION

Polymer brushes are tethered macromolecular coatings that are used to stabilize colloids 1,2 or endow surfaces with protein resistance,^{3,4} biocompatibility,^{5,6} or boundary lubrication.^{7,8} Brushes are often prepared by grafting from surfaces because this strategy produces high grafting densities desired for many applications. The main alternative to grafting from is grafting to, where pre-assembled macromolecules adsorb to an interface. At the cost of lower grafting density, 10 grafting to can produce brush coatings for many applications where grafting from is infeasible, such as in vivo coating of biosurfaces. Many highly functional coatings are produced in nature by grafting to or adsorption of bottlebrush-like glycoproteins, 11 such as lubricin 12-14 and aggrecan. 15 While these naturally occurring bottlebrushes inspire the design of novel, biomimetic surface coatings, 16-20 the optimization of these surface coatings is currently limited by a poor understanding of polymer surface conformation and adsorption kinetics.

Here, we limit our discussion to polymers bearing a single, high surface-affinity headgroup because of their structural similarity to the biological systems that inspired us. While we are primarily interested in bottlebrush end-grafting, we draw comparisons to the more extensively studied system of end-grafted linear polymers.^{21–33} In these studies, nonspecific physisorption is countered by using highly specific and strong

surface coupling chemistry, such as gold—thiol^{23–29} or amine—epoxide. ^{30–33} Linear polymers generally have three main regimes of adsorption kinetics: a transport-limited regime (I), a pause (II), and a penetration-limited regime (III). At low grafting densities, high surface affinity polymers adopt pancake-like conformations, while low surface affinity polymers adopt mushroom-like conformations. ²⁵ The onset of the pause regime is typically attributed to a mushroom-to-pancake or pancake-to-mushroom transition. These coatings typically end in the brush regime, where polymer chains overlap.

While there is a wealth of information on grafting to of linear polymers, we could not find comparable work on bottle-brushes. Synthetic bottlebrush architectures uniquely afford a high degree of control over polymer dimensions without changing the polymer's chemical identity. Specifically, the polymer's bristle length can be changed to tune the bottlebrush's Kuhn length $^{42-45}$ and excluded volume interactions for specific applications. While bottlebrushes are

Revised: November 22, 2019 Revised: February 26, 2020 Published: February 27, 2020





expected to follow qualitatively similar grafting behavior to linear polymers, we anticipate that their comparatively long side chains will exaggerate the aspects of the adsorption process associated with polymer excluded volume.

Bottlebrushes inherently have more structural parameters than linear polymers. While this makes bottlebrushes more customizable, it is difficult to exploit their mutability for grafted surface coatings without knowing how their design parameters impact their adsorption behavior. Currently, the relationships between bottlebrush dimensions and grafting behavior are poorly understood. The closest prior studies prioritized lubrication 16,18,19,46 or antifouling 20 over the fundamental phenomena underlying adsorption.

In this paper, we report on the relationships between bottlebrush polymer dimensions and the properties of the coatings they form through specific, end-functional adsorption to model surfaces. Specifically, we look at the effects of bristle and backbone lengths on bottlebrush adsorption kinetics, conformation, and antifouling properties. We find that longer bristles reduce molar adsorption, adsorption rates, brush stiffness, and antifouling ability. While increasing backbone length leads to similar trends, the effects are less dramatic than changing the bristle length.

■ MATERIALS AND METHODS

Here, we provide information on key procedures. See Supporting Information for additional details and a comprehensive list of materials, instrumentation, synthetic procedures, data analysis, and associated refs. ^{47–49}

Materials. Acetone (99.5%, Sigma-Aldrich), biotin (99%, Sigma-Aldrich), biotin-labeled bovine serum albumin (biotin-BSA, 80% protein, 8-16 biotin per protein, Sigma-Aldrich), biotin-PEG₁₀thiol (788.0 Da, 97%, Polypure), ethanol (EtOH, absolute, KOPTEC), hydrogen peroxide (35%, BDH Chemicals, for piranha), poly(ethylene glycol) thiol (PEG7-thiol, has -OH and -SH termini, 386.5 Da, 97%, Polypure), potassium chloride (99.995%, Alfa Aesar), potassium phosphate monobasic (99.8%, J.T. Baker), sodium chloride (99%, Macron Chemicals), sodium dodecyl sulfate (SDS, 99%, Sigma-Aldrich), sodium phosphate dibasic (99%, Sigma-Aldrich), streptavidin (from Streptomyces avidinii, 13 U/mg, 65-100% protein, Sigma-Aldrich), and sulfuric acid (95%, EM Science) were purchased and used as received. Biotinylated bottlebrushes were produced following adapted literature procedures⁵⁰ and characterized by NMR, gel permeation chromatography (GPC), sodium dodecyl sulfate polyacrylamide gel electrophoresis (SDS-PAGE), and Fourier transform infrared-attenuated total reflectance (FTIR-ATR) (results in Supporting Information). We manually prepared phosphate-buffered saline (PBS) using Milli-Q-grade water (18.2 MΩ·cm). See Supporting Information for a full listing of materials.

Biotin Self-Assembled Monolayer Preparation. This procedure applies for gold-coated silicon chips for atomic force microscopy (AFM), 5 MHz gold-coated sensors for quartz crystal microbalance (QCM), and sensors for localized surface plasmon resonance (LSPR, 50 or 100 nm diameter Au nanoparticles). Sonication was performed at 50 °C for 5 min and omitted for LSPR sensors. Gold-coated surfaces were rinsed with water and 1% SDS solution, sonicated in 1% SDS solution, rinsed with water, sonicated in water, rinsed with water, rinsed with acetone, rinsed with ethanol, sonicated in ethanol, rinsed with ethanol, blown dry with nitrogen gas, and placed in a glass dish. Acidic piranha solution was freshly prepared by adding 1 mL of 35% H₂O₂ solution to 3 mL of concentrated sulfuric acid and dropped onto the polished gold surfaces. After 5 min, the dish was filled with water to dilute the piranha, and chips were rinsed copiously with water, rinsed with ethanol, and blown dry with nitrogen gas. Within 5 min, the sensor surfaces were cleaned with O2 plasma at medium power for 2 min. The sensors were immediately immersed into an ethanolic solution of HO-PEG7-thiol (0.99 mM, 11.5 mg/30 mL,

99 equiv) and biotin– PEG_{10} –thiol (0.01 mM, 0.236 mg/30 mL, 1 equiv) and incubated at room temperature for 1–4 days. Chips were then rinsed with ethanol, sonicated in EtOH at 20 °C for 5 min, rinsed with ethanol, and blown dry with nitrogen gas. Polished gold surfaces were checked by ellipsometry and contact angle goniometry against water to ensure consistent and clean surfaces.

Quartz Crystal Microbalance. QCM sensors were rinsed with ethanol and blown dry with nitrogen before loading into a QCM chamber. A peristaltic pump flowed solution through the QCM cells at steady rate (0.1 mL/min \pm 10%, measured gravimetrically), while the temperature was maintained at 25 °C. The frequencies of each overtone (n = 1, 3, 5, 7, 9, 11, and 13) were found after the chambers were filled with PBS. For most experiments, the order of fluids over the QCM sensors were as follows: (1) air, (2) PBS, (3) streptavidin (25 μ g/mL in PBS, 10 min), (4) PBS, (5) bottlebrush polymer analyte (50 μ g/mL in PBS, ~1 h), (6) PBS, (7) biotin–BSA (100 μ g/ mL in PBS, 10 min), (8) PBS, (9) H₂O, and (10) air. Exceptions were made for control experiments. After the experiment, the chips were rinsed with water and blown dry with nitrogen gas prior to characterization. For simplicity, data are reported as mass densities determined by the Sauerbrey equation with a Sauerbrey constant of approximately 1.064 Da Å⁻² Hz⁻¹. We report normalized frequency shifts as $\Delta f = \text{shift/mode number}$.

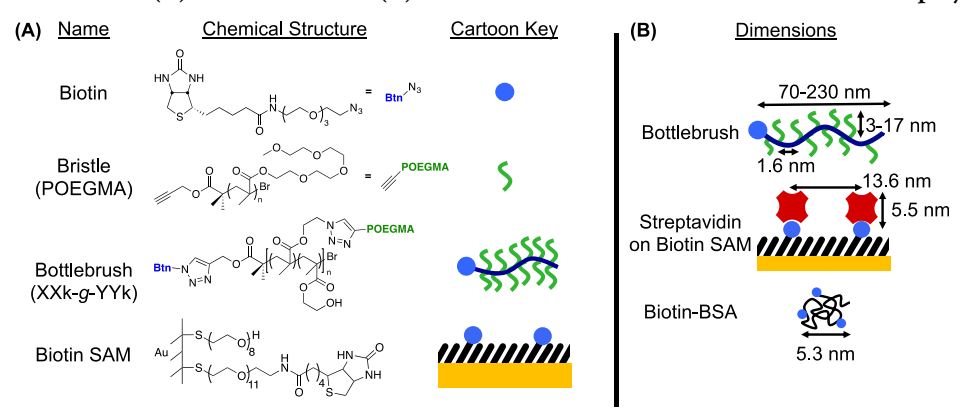
Localized Surface Plasmon Resonance. Our LSPR system maintained a constant flow of PBS over sensors at $20~\mu\text{L/min}$. The flow of buffer was interrupted with various injections that each exposed the sensor surface to an injected solution for exactly 4 min. In order, the following solutions were added across several injections: (3–10 injections) 80% isopropyl alcohol, (2 injections) streptavidin (25 μ g/mL in PBS), (3–11 injections) bottlebrush analyte (50 μ g/mL in PBS), (1 injection) biotin–BSA (100 μ g/mL in PBS), and (1 injection) water. For clarity, times between polymer injections are omitted (see Figure S54). Polymer injections were continued until the increase of polymer mass from an injection was indistinguishable from drift. Experiments with the same polymer used the same number of injections.

Atomic Force Microscopy. Briefly, we used a micromanipulator to adhere microspheres (5 μ m radius, borosilicate) to the ends of triangular, tipless AFM cantilevers (NP-OW, Veeco, cantilever B, listed spring constant 0.06–0.12 N/m). The microsphere's working side was coated with 2 nm of chromium (adhesive layer), 10 nm of gold, and a biotin self assembled monolayer (SAM). Immediately before use, biotinylated probes were rinsed with ethanol, incubated in streptavidin solution, rinsed with PBS, and incubated with a biotin–BSA solution. AFM was performed in 1% PBS solution. The probe's invOLS and spring constant were calibrated by force curves against a plain biotin–SAM surface and thermal tune. Then, force curves were acquired in 1% PBS solution at various speeds on biotinylated gold chips with streptavidin exposed to either biotin, bottlebrush, or nothing. We estimate the contact radius as the geometric mean of probe radius and double the streptavidin height.

■ RESULTS AND DISCUSSION

Experimental Design. For this study, we chose an experimental design to isolate the effect of bottlebrush dimensions on adsorption. We selected streptavidin—biotin chemistry to mediate grafting to because streptavidin—biotin coupling is strong, specific, and fast. This speed ensures that our adsorption kinetics is dominated by the bottlebrush. Additionally, streptavidin has a 5.5 nm diameter, amking it far smaller than our bottlebrushes ($R_{\rm g} > 40$ nm by SLS). We chose to use poly(oligoethylene glycol methacrylate) (POEGMA) as bristles in our bottlebrushes because POEGMA is antifouling, hydrophilic, uncharged, chemically inert, and easily prepared. Most importantly, our initial experiments showed POEGMA-based bottlebrushes have negligible nonspecific adsorption to streptavidin-modified surfaces (Figure 1B). This ensures that we only measure specific bottlebrush

Scheme 1. Chemical Structures (A) and Dimensions (B) of Macromolecules and Surface Structures Employed in This Study^a



^aStreptavidin and BSA dimensions were determined from crystal structures (1VWA⁵¹ and 3V03⁵²).

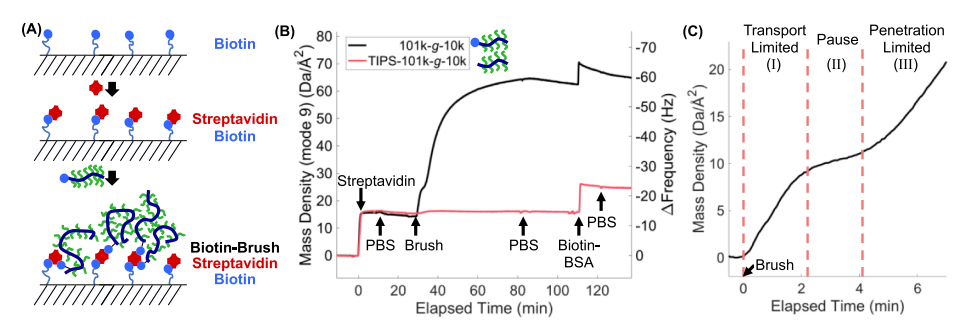


Figure 1. General experimental design (A) and representative QCM data (B,C). (B) A biotinylated sensor is exposed to $25 \,\mu\text{g/mL}$ streptavidin in PBS to form a streptavidin monolayer. A bottlebrush coating is then formed by exposure to $50 \,\mu\text{g/mL}$ biotin-bottlebrush (black) or biotin-free bottlebrush (red) by biotin-streptavidin coupling. The antifouling properties of the coating are then tested with a $100 \,\mu\text{g/mL}$ biotin-BSA solution. PBS (buffer) is flowed between solutions. Arrows indicate times when the solutions are changed. For simplicity, QCM mass density is calculated by the Sauerbrey equation. The shaded region is expanded in C with time measured from the beginning of brush adsorption. (C) Biotinylated bottlebrushes show three adsorption regimes: a transport-limited (I), a pause (II), and penetration-limited regime (III).

adsorption. Together, these features allow us to attribute differences in adsorbed layer properties to bottlebrush dimensions, making our findings more generally applicable to bottlebrush polymers.

We used our previously reported synthetic methods to prepare biotin-modified bottlebrushes by click chemistry.⁵ Specifically, we used poly(2-aminoethyl methacrylate-cohydroxyethyl methacrylate) (P(AMA-co-HEMA)) as a backbone scaffold to which we coupled a single biotin headgroup and grafted many POEGMA bristles (Scheme 1A). Our grafting to approach of bottlebrush synthesis enables us to produce a library of bottlebrushes that contains pairs of entries that differ in either backbone or bristle molecular weight. Coupled with a consistent grafting efficiency (Table S6), differences between samples are entirely attributable to backbone and bristle lengths with minimal influence from molecular weight inaccuracies or bristle spacing. Throughout this paper, we will refer to our biotinylated bottlebrushes with the abbreviation XXk-g-YYk, where XX and YY are the number average molecular weights in kDa of the backbone (by GPC) and bristle (by NMR), respectively. Negative control brushes with a triisopropyl-silyl (TIPS) protecting groups instead of biotin are abbreviated as TIPS-XXk-g-YYk.

Using gold—thiol chemistry, we prepared mixed biotin—SAMs with PEG—thiol filler using a feed ratio optimized for streptavidin binding. ⁵⁵ In our experiments, we then generated a streptavidin monolayer by exposing a biotinylated surface to streptavidin solution in PBS (Figure 1A,B). Next, we grafted

bottlebrushes to the streptavidin by flowing a biotin-bottlebrush solution (in PBS) over the surface. Lastly, we tested the antifouling properties of the coating by challenging with biotin—BSA, which has a very high affinity for streptavidin. We confirmed the chemical identity of our surface coatings by FTIR—ATR (Figure S33). Particularly, the C=O ester peak is specific to our synthetic polymer, where proteins (streptavidin and biotin—BSA) show amide I and amide II peaks at 1650 and 1550 cm⁻¹.⁵⁶

These processes were monitored in real time by LSPR with 50 and 100 nm diameter gold nanoparticles and by QCM. This combination has various advantages. First, QCM and LSPR are based on different physical principles (by acoustics and optics respectively), allowing us to validate our results through the use of these orthogonal methods. Furthermore, this combination of techniques allows us to investigate the nature of the adsorbed bottlebrushes at various length scales. Specifically, 50 and 100 nm gold particles have EM decay lengths of approximately 9 and 20 nm, respectively. In contrast, QCM acoustic waves penetrate 200 nm into aqueous solution.⁵ Thus, LSPR with 50 nm Au primarily shows signals for polymer immediately near the surface, LSPR with 100 nm Au will be medium range, and QCM will show the whole brush. Lastly, in contrast to planar QCM sensors, LSPR can also reveal curvature effects. This combination of methods allows us to both validate our findings and further investigate the structure of the bottlebrush layer.

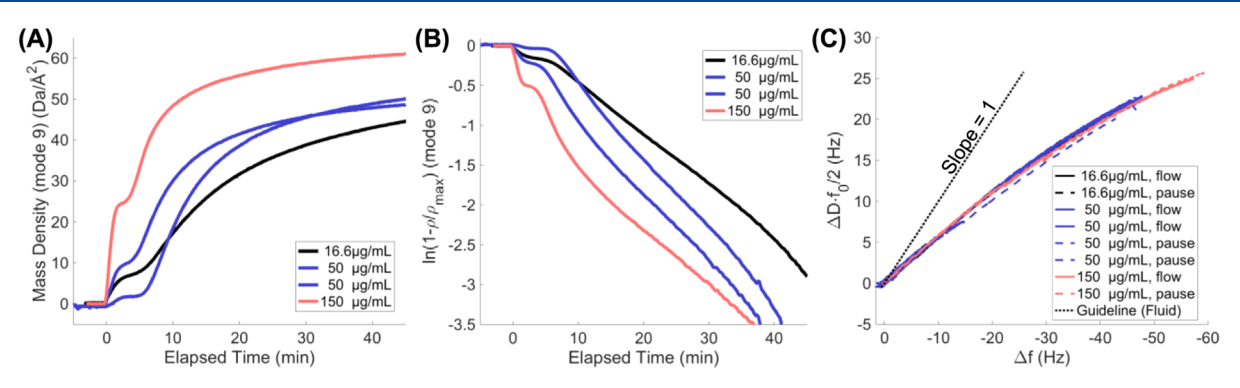


Figure 2. Effect of concentration on adsorption of 101k-g-10k onto streptavidin in PBS measured by QCM. (A) Adsorbed areal mass density (ρ) vs time calculated by the Sauerbrey equation. Zero elapsed time is defined as the time at which each polymer solution first reaches the sensor. (B) Log-transformed fractional areal mass density $(\ln(1-\rho/\rho_{\rm max}))$ plotted vs time. (C) QCM dissipation versus frequency plot showing the evolution of viscoelastic properties throughout adsorption. Curves are shown for adsorption with a constant flow of polymer solution (solid) and intermittently paused flow (dash). A dotted guideline is shown for the theoretical slope corresponding solely to a shift in fluid density and viscosity.

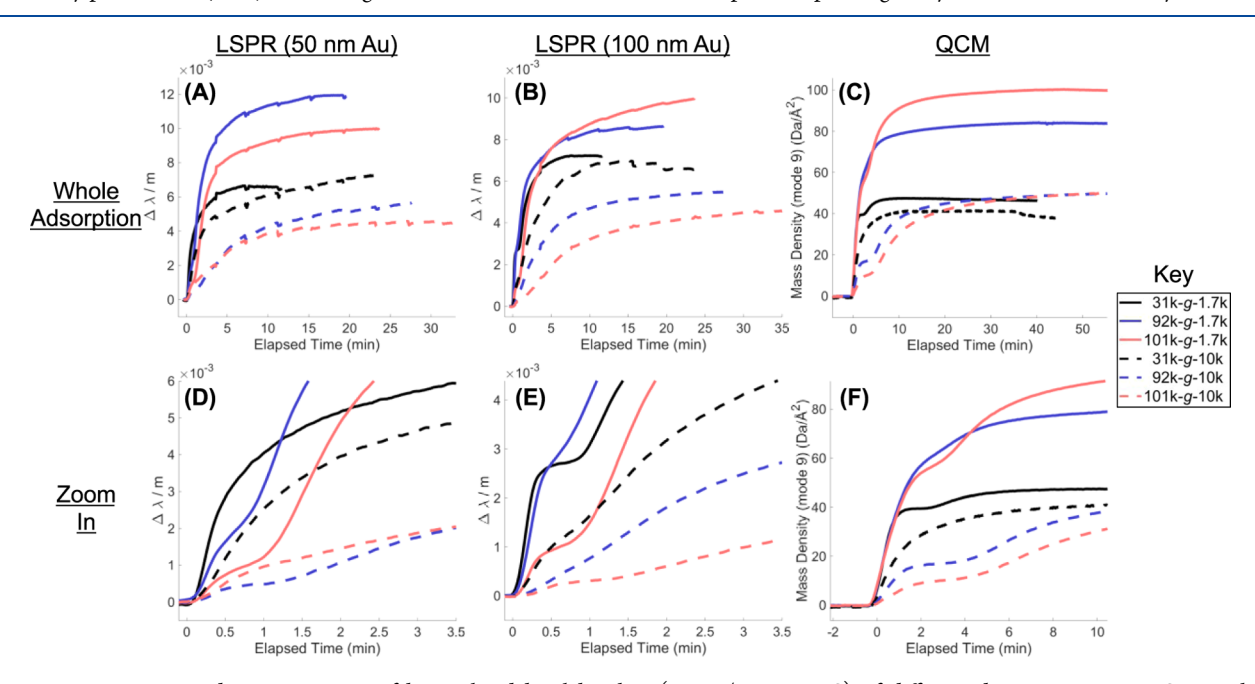


Figure 3. Representative adsorption curves of biotinylated bottlebrushes (50 μ g/mL in PBS) of different dimensions using LSPR with gold nanoparticles of 50 nm (A,D) or 100 nm diameter (B,E) and QCM (C,F). Full adsorption curves (A–C) are accompanied with a zoom-in of the first minutes of adsorption (D–F), shaded in gray. LSPR shifts ($\Delta\lambda$) are normalized to the bulk refractive index sensitivity (m) of each sensor. Data for replicates are available in Supporting Information (Figure S38).

Bottlebrush Adsorption. In most of our experiments, biotinylated bottlebrushes show three adsorption regimes: (1) a transport-limited regime, (2) a short pause, and (3) a penetration-limited regime (see Figures 1C, 2, 3). This observation is consistent with previous theoretical²¹ and experimental^{22,23,25,30–33} works on grafting kinetics for linear polymers. For our system, this behavior is absent in linear polymer controls, which quickly saturate the surface (Figures S43 and S56). Here, we will qualitatively discuss several aspects of the adsorption process of our bottlebrushes: (1) specificity, (2) kinetics, (3) conformation, and (4) mechanical properties.

Specificity. Our experiments show that our bottlebrush adsorption is extremely specific (Figure 1B). Across all experiments, only biotinylated macromolecules showed substantial adsorption, including biotinylated bottlebrushes, linear biotin—POEGMA, and biotin—BSA. In contrast, biotin-free macromolecules all showed negligible adsorption (within

noise), including control bottlebrushes and BSA. This indicates nonspecific adsorption is mostly absent in our system. Additionally, we found that the presence of streptavidin aids in blocking nonspecific adsorption beyond that provided by the PEG-rich SAM (Figure S45).

Adsorption Kinetics. The different regimes of bottlebrush adsorption kinetics mirror those of linear polymers. In the earliest stages of adsorption, surface-bound polymers adopt mostly noninteracting, mushroom-like conformations. For linear polymers, this first regime is limited by mass transport of polymer to the surface. Under flow, transport-limited kinetics follow ²¹

$$\rho(t) \approx \frac{\phi}{L_{\rm c}} \sqrt{D \ t} \tag{1}$$

where ρ is the areal mass density of polymer, t is the time, φ is bulk solution volume fraction, D is diffusivity, and L_c is contour length. This relationship means that adsorption data are

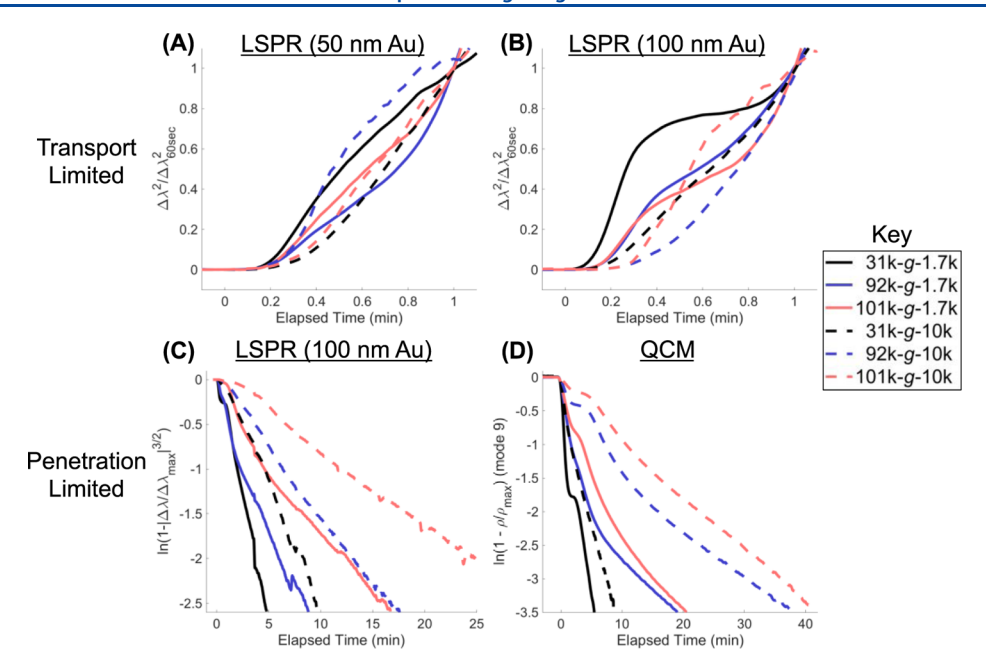


Figure 4. Adsorption kinetics of biotinylated bottlebrushes of various dimensions by LSPR (A–C) and QCM (D). 50 μ g/mL polymer solutions reach the sensors at zero elapsed time. (A,B) For times before the pause, data are linear in $\Delta\lambda^2$ vs time. These plots are normalized to shifts at 60 s for clarity. (C,D) The transformation of the *y*-axis linearizes data at times after the pause. These transformations correspond to eqs 1 and 2 for transport-limited and penetration-limited kinetics, respectively. See Figure S47 for sample fits.

linearized when plotted as ρ^2 versus t, which we observed for our bottlebrushes in regime I (Figure 4A,B). Therefore, the first kinetic regime for bottlebrush adsorption primarily follows transport-limited kinetics. When applicable, we report the root of the slope (proportional to $D^{1/2}\varphi/L_{\rm c}$) as the transport rate. To ensure that differences between slopes solely reflect changes in polymer dimensions, we kept φ constant across adsorption experiments. We found that heavier polymers exhibited smaller transport rates, which we attribute to slower diffusion.

For linear polymers, the transport-limited regime is typically followed by a latent period (pause) characterized by minimal adsorption. The adsorption kinetics of these polymers are generally modeled as a combination of Brownian diffusion and reptation-based penetration. As these mechanisms alone do not produce a pause, the pause is instead attributed to a conformational change in the brush layer. By the same logic, we reason that the pause observed during the adsorption of our bottlebrushes also originates from a conformational change. As the kinetics of the conformational change are likely specific to the polymer—surface combination, we instead focus our efforts on elucidating the nature of the conformations that define the pause, which is more generally applicable (see the Pause Conformation Section).

For linear polymers, the third regime follows penetrationlimited kinetics of the form

$$\ln\left[1 - \frac{\rho}{\rho_{\text{max}}}\right] = kt \tag{2}$$

where ρ_{max} is the maximal areal mass density and k is the rate constant. After the pause regime, our bottlebrushes closely follow this linear relationship (Figure 4C,D) and yield similar slopes (rate constants) across experiments with the same bottlebrush (Figure 2B). Whereas the model predicts a zero time intercept, our data show time offsets that directly

correlate with the variable amount of polymer present at the pause (Figure 2B). We conclude that adsorption in the late stages is penetration-limited, but simply delayed depending on the amount of mass adsorbed during the transport-limited stage.

Penetration-limited rate constants are generally smaller for bottlebrushes with longer bristles and/or backbones (Figure 5). However, increasing polymer dimensions has the biggest

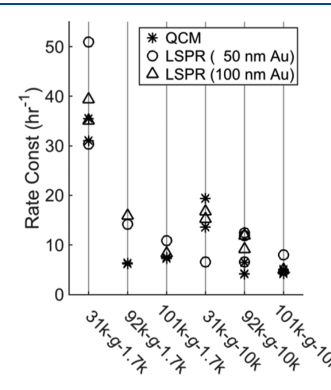


Figure 5. Rate constants of different biotinylated bottlebrushes adsorbing to streptavidin in the penetration-limited regime from 50 μ g/mL solution in PBS.

impact on rate when all of the dimensions are small. For example, increasing bristle length decreases penetration rates in polymers with 31 kDa backbones more than those with 92 kDa backbones. In contrast, the penetration rates of the bottlebrushes with the biggest backbones (101 kDa) are insensitive to the bristle length. These observations are in line with Ligoure's predictions, where penetration rate scales roughly as $\frac{\exp(-\text{const }L_cb^3)}{L_cb^4}$. We thus confirm that our bottle-brushes follow penetration-limited kinetics in the third regime consistent with the reptation-based mechanism.

Steady State Polymer Conformation. Here, we examine three features of the conformation of the polymer layer at steady state: (1) chain overlap, (2) the relationship between excluded volume interactions and bottlebrush dimensions, and (3) the occupation of space at the surface of the substrate.

We found that higher solution concentrations of biotinylated bottlebrush led to higher surface densities at steady state (Figure 2A). As higher chemical potentials can drive higher adsorption, streptavidin sites are still available at saturation. We observed that the surface density of streptavidin varies between experiments (relative deviation: QCM = 21.7%, LSPR 50 nm = 15.3%, LSPR 100 nm = 19.7%). Despite this, the final amount of adsorbed bottlebrush varied by far less across duplicate experiments ($\sim 6\%$). This implies that the grafting process is ultimately limited by excluded volume interactions that lead to a fixed surface concentration independent of the streptavidin surface density. This suggests that our bottlebrush layers are in a brush regime, even if the chains are not fully extended.

We tested the effects of the bottlebrush dimensions on the packing in the polymer layers by varying the molecular weights of the backbone and bristles, respectively (Figure 3). To isolate the effects of polymer dimensions, we maintained the same polymer chemical potentials across samples by maintaining polymer mass concentration in solution constant. Increasing any bottlebrush dimension increases molar mass and decreases surface molar grafting density, typically attributed to excluded volume interactions. \$9,60 Adsorbed mass is the product of molar mass and molar grafting density. We observe that longer backbones give higher adsorbed masses because the increase in each polymer's molecular weight exceeds the ensuing reduction in molar grafting density. In contrast, longer bristles lead to lower total mass because the excluded volume interactions scale more strongly with bristle molecular weight. Furthermore, the longer a bottlebrush's bristles were, the more sensitive was its molar grafting density to changes in backbone length. These observations are all consistent with a steric gating of the grafting process during the penetration-limited regime. In this regime, adsorption is limited by a polymer's pervaded volume, which scales more heavily with Kuhn length than with contour length. While there is a debate on how intensely bristle length increases Kuhn length, 42-45,61 our system clearly shows that an increase in bristle length leads to more volume exclusion than it leads to molar mass amplification. This is in contrast to the effects of backbone length, which has a greater impact on molar mass than on volume exclusion.

To interrogate the brush at the interface, we probed the distribution of mass at the base of the layer by using LSPR sensors of different decay lengths (see Supporting Information for details). As a proof of concept, we determined the thickness of streptavidin coatings by their relative sensor ratio responses. We modeled the streptavidin layer as a collection of cylinders of height *H* to simulate each protein's pervaded volume. In this model, the ratio between the LSPR sensor responses is given by

$$\frac{\Delta \lambda_9 m_{20}}{\Delta \lambda_{20} m_9} = \frac{1 - e^{-2H/l_9}}{1 - e^{-2H/l_{20}}} \tag{3}$$

where subscripts denote each sensor's decay length in nm, $\Delta\lambda$ is the LSPR shift, m is the sensor sensitivity, and l is the decay length. We measured $\Delta\lambda_9 m_{20}/\Delta\lambda_{20} m_9 = 1.69 \pm 7.7\%$ (SE) for streptavidin layers. This yields a calculated streptavidin layer

thickness of 5.3 ± 1.6 nm, which is close to the expected 5.5 nm (crystal structure 1VWA⁵¹). This gives us confidence to analyze the bottlebrush–substrate interface with this technique.

We calculate that $86.8 \pm 0.65\%$ (relative SE) of the streptavidin layer's volume is unoccupied. Thus, we have two hypotheses about how the brush occupies this free space. Bottlebrushes either fill the volume between surface-bound streptavidin or they do not. We calculated $\Delta \lambda_9 m_{20} / \Delta \lambda_{20} m_9 =$ 1.03-1.31 from measurements of our six biotinylated bottlebrushes at equilibrium. We interpreted this result by modeling the system as a polymer brush layer with a parabolic segment density profile. 62 For the case where the bottlebrush does not fill the volume between surface-bound streptavidin, this density profile is separated from the surface by an empty 5.5 nm layer (see Figure S4). This model leads to brush heights of 19-70 nm if bottlebrushes fill the space between streptavidin or heights of -2.9 to 2.2 nm if they do not. As individual macromolecules are larger than 10 nm, we conclude that our bottlebrushes occupy the space between streptavidin regardless of bottlebrush dimension.

Pause Conformation. To understand the polymer conformation during the pause, we examine three aspects of the adsorption process during the pause: (1) molecular weight dependence, (2) polymer mass redistribution, and (3) variability in the pause onset. The pause in the adsorption process is extremely sensitive to polymer dimensions (Figure 3D-F). Generally, larger bottlebrushes exhibit more pronounced pauses that occur at lower adsorption relative to steady state. Surprisingly, the pauses for the lowest aspect ratio (backbone/bristle) bottlebrush (31k-g-10k) were the least pronounced (or totally absent) across techniques. However, polymers sharing a common length (31k backbone or 10k bristle) show strong pauses in medium-long decay length techniques (100 nm Au LSPR and QCM) that more accurately measure the total adsorbed amount. As bristle length increases Kuhn length, this observation implies that the behavior characterizing the pause regime involves backbone rearrangement because a pause is only observed for higher aspect ratio bottlebrushes.

We find that the smallest bottlebrush (31k-g-1.7k) shows a strong pause in adsorption when observed in medium-long decay length techniques, but this pause is surprisingly absent in our short decay length technique (LSPR with 50 nm Au). If this observation were simply caused by a curvature effect (50 vs 100 nm Au nanoparticles), then all the other bottlebrushes would have been even more sensitive to curvature because they are larger (lower $R_{\text{particle}}/R_{\text{polym}}$).⁶³ We thus attribute this observation to the difference in decay lengths of the sensors (9 vs 20 nm EM decay length). Because the medium-long decay length techniques observe the brush layer more completely, the pause in these techniques is indeed a pause in the total adsorbed mass. However, the short decay length sensor mostly sees the base of the brush, and it registers a constantly increasing signal. Taken together, we conclude that polymer mass generally stays constant during the pause, but redistributes itself closer to the substrate (see Extended Discussion in Supporting Information for discussion on other

While polymer adsorption ultimately ends with a consistent steady state surface density, the amount of polymer present at the pause regime is quite variable across duplicate experiments (Figures 2A and S38). However, the amount present at the

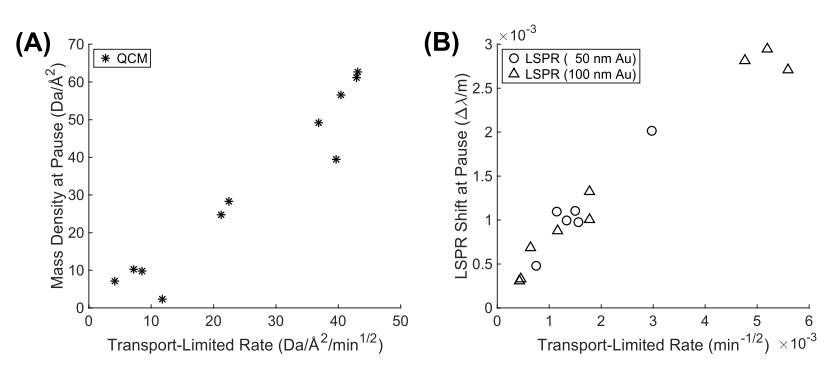


Figure 6. Relationship between the adsorbed mass at the pause and the transport-limited rate for biotinylated bottlebrush coatings of various molar masses in (A) QCM and (B) LSPR. This includes all samples from Figures 2A, 3, S38 and S57 with clear pause regimes.

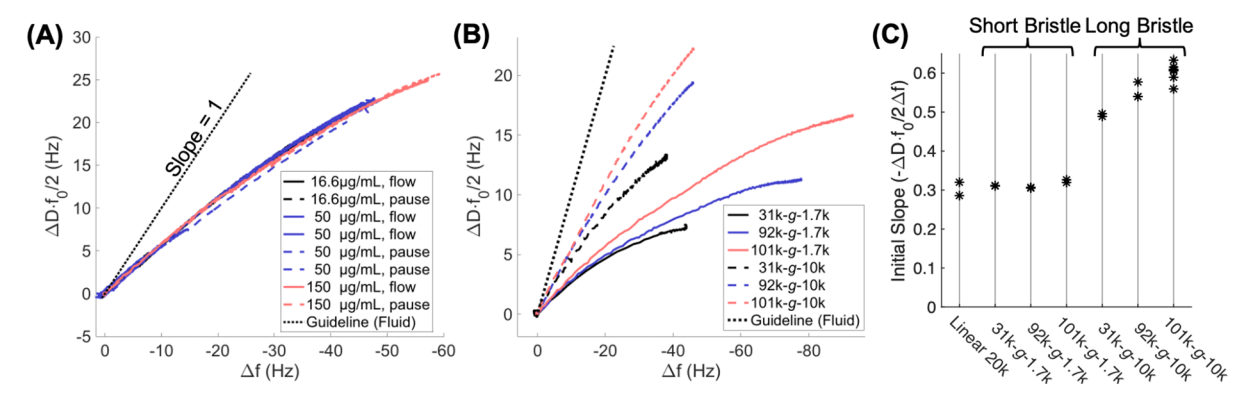


Figure 7. Dissipation vs frequency data for the adsorption of biotinylated bottlebrushes by QCM (9th overtone). (A) 101k-g-10k adsorbed at various concentrations under a constant flow (flow) or intermittently paused flow (pause). (B) Different bottlebrushes adsorbed from 50 μ g/mL solutions. For reference, a dotted guideline shows the response expected for a Newtonian fluid. (C) Each analyte showed a different initial slope in its dissipation vs frequency plot. Data for linear biotin–POEGMA ("linear 20k") is shown for comparison. Each sample has at least two data points.

pause positively correlates with the mass transport rate across many experiments (Figure 6, see eq 1) and occurs whether the solution flows or stagnates (Figures S50 and S51). In the limiting case of high transport-limited rates (achievable with high polymer concentrations), we expect the pause to disappear, which is consistent with literature reports.²³ Prior works on linear polymer adsorption have attributed the pause to a mushroom-to-brush^{22,23,26,30,32} or pancake-to-brush^{25,64,65} transition, occurring at the overlap concentration. If the surface conformation were solely a state function of areal mass density, then overlap would be observed at the same areal mass density every time the experiment is run. However, because our bottlebrushes have variable mass densities at the pause, we conclude that the polymer conformation is not a state function of areal mass density in our system.

Thus, we attribute the variability in the onset of the pause regime across duplicate experiments to differences in streptavidin binding capacity and minor differences in the polymer concentration near the surface. Specifically, the amount of polymer present during the pause is proportional to the variable rate of polymer transport to the surface during the first regime. This suggests that the polymers in the layer require a fixed amount of time to rearrange to a surface-induced conformation that blocks access to streptavidin. This rearrangement defines the onset of the pause, which is governed by a characteristic time and not a characteristic areal mass density, as observed experimentally. From experiments where we varied bottlebrush dimensions, we have already concluded that polymer segment density shifts closer to the surface during the pause. Based on this evidence, we

infer that the pause regime likely originates from a mushroom-to-pancake transition caused by a weak interaction between the polymer and the SAM on the substrate surface. This notion of a weak interaction is consistent with our bottlebrushes pausing for less than 5 min while more surface-adhesive brushes can stay paused for over a day²⁵ because in the latter case, the polymer segments take more time to dissociate from the substrate.

In conclusion, the pause regime of our bottlebrushes is characterized by a surface-induced rearrangement of polymer toward the surface that is independent of grafting density and requires backbone reorganization. We attribute this rearrangement to a mushroom-to-pancake transition.

Mechanical Damping Properties of the Bottlebrush Coating. In addition to measuring mass, QCM can also measure the dissipation of acoustic energy of an adsorbed layer. In Figure 7, we plot the ratio between dissipation (ΔD) and normalized frequency response (Δf = frequency shift/mode number) scaled by the fundamental resonant frequency (f_0). This enables us to monitor a polymer layer's specific dissipation ($-\Delta D f_0/2\Delta f$, dissipation per mass) as it forms. In a dissipation versus frequency plot, a Newtonian fluid with changing density or viscosity produces a slope of one. Furthermore, the growth of a thin, homogeneous film will produce a straight line with a slope that is characteristic of the material's mechanical damping properties. Specifically, smaller slopes indicate materials with less mechanical loss (i.e., they are less viscoelastic).

We find that biotinylated bottlebrushes produce extremely reproducible dissipation versus frequency responses despite the different concentrations or intentionally paused flow rates (Figure 7A). Additionally, there is no discernable kink in the plot that could be associated with the pause regime. This is in contrast to PNIPAM brushes grafted to gold, which have a clear change of slope (0.075-0.325) at their pancake-to-brush transitions. Thus, our observations indicate that the dissipative properties of our bottlebrush layers are mostly independent of polymer conformation. Additionally, each sample shows a decreasing slope in its D/f response as more bottlebrushes fill the layer (Figure 7B). This mild downward concavity indicates a stiffening of the brush layer, which we attribute to denser brush packing. This is in contrast to nonspecific adsorbers, which generally show D/f responses with upward concavities 66,67 as adsorbers bind to the surface more loosely late into the adsorption process.

Our data also show that longer bristles dramatically increase a brush layer's specific dissipation (Figure 7B,C). While increasing backbone length also increases specific dissipation, the magnitude of this effect is much weaker than that for bristles. Interestingly, backbone length has a bigger impact on brush mechanical properties for bottlebrushes with longer bristles than those with shorter bristles (Figure 7C). We explain this result by the differences in flexibility of these polymers. As the number of Kuhn segments in the bottlebrush scales with its aspect ratio, we hypothesize that having more Kuhn segments increases the specific dissipation of the polymer layer up to a point. Specifically, the flexibility of the backbone contributes to the specific dissipation of the layer as a whole.

Our brush layers have high specific dissipations $(-\Delta D f_0/2\Delta f = 0.3-0.6)$. To put this into context, POEGMA brushes grown by SI-ATRP give $-\Delta D f_0/2\Delta f = 0.16$ for dense brushes⁶⁸ and $-\Delta D f_0/2\Delta f = 0.62$ for more swollen brushes⁶⁹ (5% polymer by volume). Thus, our bottlebrush coatings are mechanically much closer to highly swollen brushes than densely packed brushes, which is consistent with our *grafting to* method.

Antifouling Properties of the Bottlebrush Coating. By testing the antifouling properties of our bottlebrush coatings, we investigated the effects of bottlebrush structure on both the coating's antifouling ability and its permeability to macromolecules. Specifically, we challenged our bottlebrush coatings with biotin-BSA, which has high affinity for the streptavidin base layer but empirically no affinity for POEGMA.⁶⁹ As a result, our measurements lack nonspecific interactions that are unique to a particular combination of adsorber, substrate, and polymer. Therefore, by measuring the amount of biotin-BSA that can reach the surface, we can probe the ability of bottlebrushes to exclude other macromolecules from entering the brush layer solely as a function of polymer dimension. We conservatively estimate that <50% of streptavidin sites are occupied by bottlebrushes (Figure S52), which means that most sites remain available for biotin-BSA adsorption in all experiments.

QCM and LSPR measurements showed that every biotinylated bottlebrush coating either reduced or totally blocked biotin—BSA adsorption (Figure S60, Table S9). Here, we focus on LSPR results because the LSPR signal is strongest near the surface where biotin—BSA would bind streptavidin, thus yielding more sensitive measurements of fouling. Our data showed that bottlebrush coatings with short bristles completely repel biotin—BSA, while longer bristles led to substantial fouling (Figure 8). Furthermore, among the long-bristle

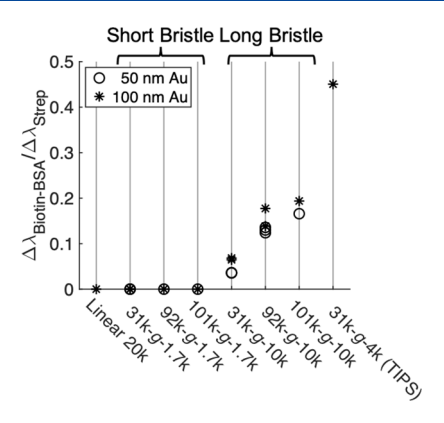


Figure 8. Biotin–BSA fouling onto bottlebrush coatings grafted to streptavidin measured by LSPR with 50 nm gold (O) and 100 nm gold (*). Fouling is normalized to the LSPR shift of streptavidin on the same sensor. Bottlebrush coatings were prepared from 50 μ g/mL PBS solutions.

bottlebrushes, a longer backbone led to increased fouling. Based on our steady state adsorbed quantities, we find that antifouling very strongly correlates with polymer grafting density, which controls excluded volume interactions. The similarity of our results across orthogonal techniques and geometries indicates that the antifouling properties of these coatings are mostly independent of the substrate's curvature.

To further test the permeability of our coatings, we prepared a coating with 92k-g-10k, then exposed it to a 50 μ g/mL solution of either linear biotin–POEGMA ("linear 20 kDa") or 92k-g-1.7k (Figures S48 and S49). In both cases, the new polymer adsorbed through the pre-existing layer without a pause regime. This adsorption shows that the bottlebrush coatings are permeable to macromolecules that are smaller than the constituent polymer. This is consistent with the findings of previous studies on linear polymers. ⁷⁰

We then investigated how the coatings prevent fouling under pressure. Briefly, we measured adhesion forces between a biotin—BSA-modified colloidal probe and streptavidin surfaces decorated with bottlebrush coatings (Figure 9). These AFM measurements complement our antifouling measurements in solution because both methods probe protein adhesion through the brush layer. However, AFM probes the adhesion after forcefully pressing biotin—BSA into the surface. This compression more accurately reflects the condition under which natural glycoprotein coatings function at biointerfaces, such as in articular cartilage. While we expect anti-adhesive properties to correlate with antifouling in solution, the addition of pressure introduces differences because of brush collapse and nonspecific interactions.

As the contact radius easily exceeds 200 nm, each pull measures multiple biotin—BSA-mediated surface interactions. This ensemble measurement allows us to probe the layer's antiadhesive properties instead of single BSA extension profiles. Our control experiments showed that the pull-off forces between biotin—BSA probes and streptavidin surfaces were much larger than the literature value of ~200 pN for a single streptavidin—biotin rupture. In contrast, streptavidin surfaces blocked with biotin showed greatly reduced pull-off forces (Figure 9C). Therefore, this technique is sensitive to specific binding while showing a small contribution from nonspecific interactions. The thin bottlebrush (101k-g-1.7k) that repelled biotin—BSA in solution also reduced biotin—BSA adhesion after applying ~30 kPa of pressure, roughly matching results

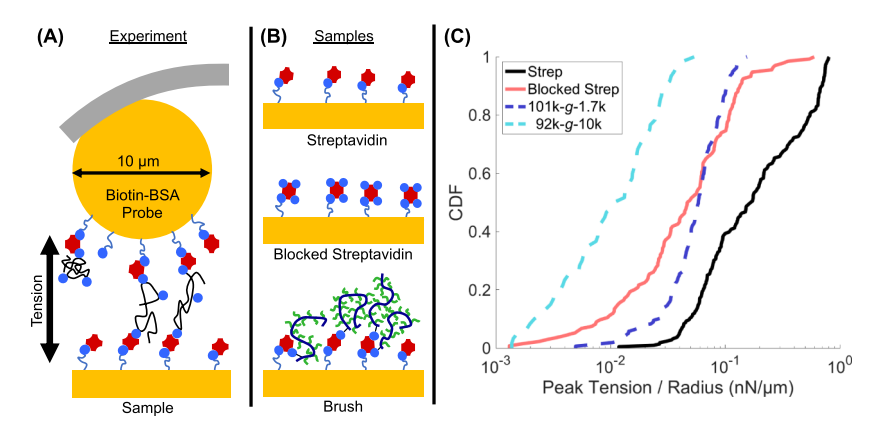


Figure 9. AFM peak pull-off forces between biotin—BSA-coated colloidal probes (8–16 biotin/BSA) and modified streptavidin surfaces. (A) In the experiment, a biotin—BSA-coated colloidal probe links to available streptavidin in the sample. Pulling away leads to tension as the BSA is pulled apart. (B) Samples for this experiment include a streptavidin surface exposed to nothing (positive control), free biotin (negative control), or biotin-bottlebrush. (C) Cumulative density functions show the distributions of peak pull-off forces measured across the experimental conditions, pooled across various probes, zones, and samples. Forces are normalized to the radius of each probe (measured by SEM). For original force curves, see Figures S62–S65.

with the blocked streptavidin. Surprisingly, the thick bottle-brush (101k-g-10k) that allowed substantial adsorption of biotin—BSA in QCM and LSPR experiments completely repelled biotin—BSA after applying pressure. Specifically, most force curves had no observable adhesion (Figure S65), reducing adhesion more than biotin blocking or short-bristle bottlebrushes. We speculate that this behavior stems from the bottlebrush blocking access to both the underlying surface and streptavidin sites more effectively when it has long bristles.

CONCLUSIONS

Guided bottlebrush adsorption (grafting to) makes it possible to form functional brush coatings on target surfaces for which grafting from strategies are infeasible. The modular design of our bottlebrushes allowed us to tune their dimensions and readily incorporate functional headgroups to specifically adhere to a target surface. We tailored our bottlebrushes to adsorb to streptavidin surfaces through biotin-streptavidin coupling. Historically, changing contour length has been the only route to change a polymer's adsorption behavior without altering its chemical composition or adsorption conditions. Bottlebrush polymers additionally allow the polymer's Kuhn length to be tuned by altering the side chain length. In this study, we aimed to elucidate the effects of bottlebrush dimensions on the properties of their layers, specifically formation kinetics, conformation, mechanical loss, antifouling ability, and antiadhesive properties. The dimensions of our bottlebrushes profoundly affected every aspect of the resulting brush layers. Generally, bristle size impacts bottlebrush adsorption properties much more than backbone length. More specifically, bristle lengths strongly influence the excluded volume interactions that govern the grafting to process. As a result, longer bristles lead to lower grafting densities (molar and mass), softer brushes, and reduced antifouling properties. In contrast, longer backbones lead to slight reductions in molar grafting density, brush stiffness, and antifouling properties, but lead to higher areal mass density. We found that bottlebrush coatings with short bristles effectively blocked fouling by biotin-BSA in solution. However, longer bristle lengths lead to greater antiadhesive properties after applying pressure. Furthermore, long bristle bottlebrushes produced coatings that were substantially more viscoelastic than those of the equivalent linear polymer.

This implies that the brush architecture substantially increases mechanical loss.

Just like linear polymers, our bottlebrush adsorption showed 3 kinetic regimes: a transport-limited regime, a pause, and a penetration-limited regime. Adsorption rate during the transport-limited regime is directly tied to polymer diffusion, which has substantial contribution from both bristle and backbone lengths. Surprisingly, this process ends after a certain amount of time and not by reaching a critical mass density. This implies that the pause regime is triggered by a conformational rearrangement of the bottlebrush that blocks surface access wherein the polymer moves closer to the surface. As a result, the variable amount of polymer present at the pause is determined by the amount of the polymer that can be transported to the surface during the preceding transportlimited regime, which depends on solution concentration, flow rates, and polymer diffusivity. The pause ends after a fixed amount of time spent with constant exposure to the polymer in solution. This indicates that the penetration-limited regime is not solely triggered by a conformational waiting period. Penetration-limited kinetics are substantially retarded if either the backbone or the bristles are long. This finding is consistent with reptation-based penetration observed in linear polymers. The penetration-limited regime is only affected by the amount of the polymer at the pause, which simply delays adsorption by a fixed time.

We found that the basic physics of bottlebrushes in grafting to is analogous to that of linear polymers. Furthermore, our observed structure-function relationships empower chemists with a better understanding of how structural parameters will influence the properties of new bottlebrush coatings. Additionally, our work helps to understand how the dimensions of biological bottlebrushes are optimized to serve specific functions. For example, lubricin is a brush-like glycoprotein that adsorbs to cartilage with its C-terminal domain. 12,72 Lubricin's brush has a relatively long backbone (91 kDa, 72,73 Genebank: NM_005807.5) and short bristles (3-6 sugar rings⁷⁴). Based on our findings, we conjecture that lubricin's dimensions are optimized for a high antifouling ability, low energy dissipation, and high mass adsorption at the cost of slightly slower adsorption. However, one must consider such conclusions cautiously because glycoproteins are typically

charged, which complicates predictions even in high ionic strength media. In summary, our findings elucidate the adsorption behavior of uncharged bottlebrushes and inform design parameters for new bottlebrush coatings.

ASSOCIATED CONTENT

5 Supporting Information

The Supporting Information is available free of charge at https://pubs.acs.org/doi/10.1021/acs.langmuir.9b03620.

Detailed materials, methods, spectra, and additional data (PDF)

Derivation of formulas for LSPR analysis (PDF)

AUTHOR INFORMATION

Corresponding Author

Stefan Zauscher — Department of Mechanical Engineering and Materials Science, Duke University, Durham, North Carolina 27708, United States; orcid.org/0000-0002-2290-7178; Email: zauscher@duke.edu

Authors

Luis A. Navarro – Department of Mechanical Engineering and Materials Science, Duke University, Durham, North Carolina 27708, United States; oorcid.org/0000-0002-7536-308X

Tejank P. Shah – Department of Mechanical Engineering and Materials Science, Duke University, Durham, North Carolina 27708, United States

Complete contact information is available at: https://pubs.acs.org/10.1021/acs.langmuir.9b03620

Author Contributions

The manuscript was written through contributions of all the authors. All the authors have given approval to the final version of the manuscript.

Funding

Funding was provided by the National Science Foundation (NSF) Triangle Materials Research Science and Engineering Center (MRSEC, DMR-1121107) and by support through NSF DMR-1729671.

Notes

The authors declare no competing financial interest.

ACKNOWLEDGMENTS

Thanks to Daniel French for preparing TIPS-92k-g-1.8k.

ABBREVIATIONS

AFM, atomic force microscopy; AMA, 2-aminoethyl methacrylate (backbone coupling monomer); BSA, bovine serum albumin; HEMA, 2-hydroxyethyl methacrylate (backbone filled monomer); LSPR, localized surface plasmon resonance; PBS, phosphate-buffered saline; POEGMA, poly(oligo-(ethylene glycol) methacrylate) (bristle polymer); QCM, quartz crystal microbalance; TIPS, triisopropylsilyl (alkyne protecting group); TIPS-XX-g-YY, XX-g-YY with TIPS instead of biotin; XX-g-YY, biotin—poly((AMA-g-POEGMA)-co-HEMA) with XX kDa backbone and YY kDa POEGMA bristles (biotinylated bottlebrush).

REFERENCES

(1) Zhao, B.; Brittain, W. J. Polymer brushes: surface-immobilized macromolecules. *Prog. Polym. Sci.* **2000**, *25*, *677*–710.

- (2) Corbierre, M. K.; Cameron, N. S.; Lennox, R. B. Polymer-stabilized gold nanoparticles with high grafting densities. *Langmuir* **2004**, *20*, 2867–2873.
- (3) Chen, S.; Li, L.; Zhao, C.; Zheng, J. Surface hydration: Principles and applications toward low-fouling/nonfouling biomaterials. *Polymer* **2010**, *51*, 5283–5293.
- (4) Krishnamoorthy, M.; Hakobyan, S.; Ramstedt, M.; Gautrot, J. E. Surface-initiated polymer brushes in the biomedical field: applications in membrane science, biosensing, cell culture, regenerative medicine and antibacterial coatings. *Chem. Rev.* **2014**, *114*, 10976–11026.
- (5) Milner, S. T. Polymer brushes. Science 1991, 251, 905-914.
- (6) Callow, J. A.; Callow, M. E. Trends in the development of environmentally friendly fouling-resistant marine coatings. *Nat. Commun.* **2011**, 2, 244.
- (7) Zhulina, E. B.; Rubinstein, M. Lubrication by Polyelectrolyte Brushes. *Macromolecules* **2014**, *47*, 5825–5838.
- (8) Kyomoto, M.; Moro, T.; Saiga, K.; Hashimoto, M.; Ito, H.; Kawaguchi, H.; Takatori, Y.; Ishihara, K. Biomimetic hydration lubrication with various polyelectrolyte layers on cross-linked polyethylene orthopedic bearing materials. *Biomaterials* **2012**, 33, 4451–4459.
- (9) Zoppe, J. O.; Ataman, N. C.; Mocny, P.; Wang, J.; Moraes, J.; Klok, H.-A. Surface-Initiated Controlled Radical Polymerization: State-of-the-Art, Opportunities, and Challenges in Surface and Interface Engineering with Polymer Brushes. *Chem. Rev.* **2017**, *117*, 1105–1318.
- (10) Barbey, R.; Lavanant, L.; Paripovic, D.; Schüwer, N.; Sugnaux, C.; Tugulu, S.; Klok, H.-A. Polymer brushes via surface-initiated controlled radical polymerization: synthesis, characterization, properties, and applications. *Chem. Rev.* **2009**, *109*, 5437–5527.
- (11) Navarro, L. A.; French, D. L.; Zauscher, S. Advances in mucin mimic synthesis and applications in surface science. *Curr. Opin. Colloid Interface Sci.* **2018**, *38*, 122–134.
- (12) Chang, D. P.; Abu-Lail, N. I.; Guilak, F.; Jay, G. D.; Zauscher, S. Conformational mechanics, adsorption, and normal force interactions of lubricin and hyaluronic acid on model surfaces. *Langmuir* **2008**, *24*, 1183–1193.
- (13) Zappone, B.; Ruths, M.; Greene, G. W.; Jay, G. D.; Israelachvili, J. N. Adsorption, lubrication, and wear of lubricin on model surfaces: polymer brush-like behavior of a glycoprotein. *Biophys. J.* **2007**, *92*, 1693–1708.
- (14) Greene, G. W.; Martin, L. L.; Tabor, R. F.; Michalczyk, A.; Ackland, L. M.; Horn, R. Lubricin: a versatile, biological anti-adhesive with properties comparable to polyethylene glycol. *Biomaterials* **2015**, 53, 127–136.
- (15) Seror, J.; Merkher, Y.; Kampf, N.; Collinson, L.; Day, A. J.; Maroudas, A.; Klein, J. Articular cartilage proteoglycans as boundary lubricants: structure and frictional interaction of surface-attached hyaluronan and hyaluronan–aggrecan complexes. *Biomacromolecules* 2011, 12, 3432–3443.
- (16) Banquy, X.; Burdyńska, J.; Lee, D. W.; Matyjaszewski, K.; Israelachvili, J. Bioinspired bottle-brush polymer exhibits low friction and Amontons-like behavior. *J. Am. Chem. Soc.* **2014**, *136*, 6199–6202.
- (17) Lawrence, A.; Xu, X.; Bible, M. D.; Calve, S.; Neu, C. P.; Panitch, A. Synthesis and characterization of a lubricin mimic (mLub) to reduce friction and adhesion on the articular cartilage surface. *Biomaterials* **2015**, 73, 42–50.
- (18) Samaroo, K. J.; Tan, M.; Putnam, D.; Bonassar, L. J. Binding and lubrication of biomimetic boundary lubricants on articular cartilage. *J. Orthop. Res.* **2017**, *35*, 548–557.
- (19) Samaroo, K. J.; Tan, M.; Andresen Eguiluz, R. C.; Gourdon, D.; Putnam, D.; Bonassar, L. J. Tunable Lubricin-mimetics for Boundary Lubrication of Cartilage. *Biotribology* **2017**, *9*, 18–23.
- (20) Xia, Y.; Adibnia, V.; Shan, C.; Huang, R.; Qi, W.; He, Z.; Xie, G.; Olszewski, M.; De Crescenzo, G.; Matyjaszewski, K.; Banquy, X.; Su, R. Synergy between Zwitterionic Polymers and Hyaluronic Acid Enhances Antifouling Performance. *Langmuir* **2019**, *35*, 15535.

- (21) Ligoure, C.; Leibler, L. Thermodynamics and kinetics of grafting end-functionalized polymers to an interface. *J. Phys.* **1990**, *51*, 1313–1328.
- (22) Zhang, S.; Vi, T.; Luo, K.; Koberstein, J. T. Kinetics of Polymer Interfacial Reactions: Polymer Brush Formation by Click Reactions of Alkyne End-Functional Polymers with Azide-Functional Substrates. *Macromolecules* **2016**, *49*, 5461–5474.
- (23) Sha, X.; Xu, X.; Sohlberg, K.; Loll, P. J.; Penn, L. S. Evidence that three-regime kinetics is inherent to formation of a polymer brush by a grafting-to approach. *RSC Adv.* **2014**, *4*, 42122–42128.
- (24) Liu, G.; Zhang, G. Grafting Kinetics of Polymer Chains. In *QCM-D Studies on Polymer Behavior at Interfaces*; Springer Science & Business Media, 2013; pp 33–44.
- (25) Liu, G.; Cheng, H.; Yan, L.; Zhang, G. Study of the kinetics of the pancake-to-brush transition of poly(N-isopropylacrylamide) chains. *J. Phys. Chem. B* **2005**, *109*, 22603–22607.
- (26) Liu, G.; Yan, L.; Chen, X.; Zhang, G. Study of the kinetics of mushroom-to-brush transition of charged polymer chains. *Polymer* **2006**, 47, 3157–3163.
- (27) Tokumitsu, S.; Liebich, A.; Herrwerth, S.; Eck, W.; Himmelhaus, M.; Grunze, M. Grafting of alkanethiol-terminated poly(ethylene glycol) on gold. *Langmuir* **2002**, *18*, 8862–8870.
- (28) Patton, D.; Knoll, W.; Advincula, R. C. Polymer Loops vs. Brushes on Surfaces: Adsorption, Kinetics, and Viscoelastic Behavior of α , ω -Thiol Telechelics on Gold. *Macromol. Chem. Phys.* **2011**, 212, 485–497.
- (29) Taylor, W.; Jones, R. A. L. Producing high-density high-molecular-weight polymer brushes by a "grafting to" method from a concentrated homopolymer solution. *Langmuir* **2010**, *26*, 13954–13958
- (30) Huang, H.; Rankin, S. E.; Penn, L. S.; Quirk, R. P.; Cheong, T. H. Transition from mushroom to brush during formation of a tethered layer. *Langmuir* **2004**, *20*, 5770–5775.
- (31) Huang, H.; Penn, L. S.; Quirk, R. P.; Cheong, T. H. Effect of segmental adsorption on the tethering of end-functionalized polymer chains. *Macromolecules* **2004**, *37*, 516–523.
- (32) Penn, L. S.; Huang, H.; Sindkhedkar, M. D.; Rankin, S. E.; Chittenden, K.; Quirk, R. P.; Mathers, R. T.; Lee, Y. Formation of tethered nanolayers: Three regimes of kinetics. *Macromolecules* **2002**, 35, 7054–7066
- (33) Penn, L. S.; Hunter, T. F.; Lee, Y.; Quirk, R. P. Grafting rates of amine-functionalized polystyrenes onto epoxidized silica surfaces. *Macromolecules* **2000**, *33*, 1105–1107.
- (34) Baekmark, T. R.; Wiesenthal, T.; Kuhn, P.; Albersdörfer, A.; Nuyken, O.; Merkel, R. A systematic infrared reflection-absorption spectroscopy and film balance study of the phase behavior of lipopolymer monolayers at the air-water interface. *Langmuir* **1999**, *15*, 3616–3626.
- (35) Wiesenthal, T.; Baekmark, T. R.; Merkel, R. Direct evidence for a lipid alkyl chain ordering transition in poly(ethylene oxide) lipopolymer monolayers at the air-water interface obtained from infrared reflection absorption spectroscopy. *Langmuir* 1999, 15, 6837–6844
- (36) Baekmark, T. R.; Elender, G.; Lasic, D. D.; Sackmann, E. Conformational Transitions of Mixed Monolayers of Phospholipids and Poly(Ethylene Oxide) Lipopolymers and Interaction Forces with Solid-Surfaces. *Langmuir* **1995**, *11*, 3975–3987.
- (37) Paeng, K.; Choi, J.; Park, Y.; Sohn, D. Temperature effect of hydrophobically modified polyethylene oxide at the air—water interface. *Colloids Surf., A* **2003**, 220, 1–7.
- (38) Tsukanova, V.; Salesse, C. On the nature of conformational transition in poly(ethylene glycol) chains grafted onto phospholipid monolayers. *J. Phys. Chem. B* **2004**, *108*, 10754–10764.
- (39) Bijsterbosch, H. D.; de Haan, V. O.; de Graaf, A. W.; Mellema, M.; Leermakers, F. A. M.; Stuart, M. A. C.; Well, A. A. v. Tethered Adsorbing Chains Neutron Reflectivity and Surface Pressure of Spread Diblock Copolymer Monolayers. *Langmuir* **1995**, *11*, 4467–4473.

- (40) Gonçalves da Silva, A. M.; Filipe, E. J. M.; dOliveira, J. M. R.; Martinho, J. M. G. Interfacial behavior of poly(styrene)-poly(ethylene oxide) diblock copolymer monolayers at the air-water interface. Hydrophilic block chain length and temperature influence. *Langmuir* 1996, 12, 6547–6553.
- (41) Gragson, D. E.; Jensen, J. M.; Baker, S. M. Characterization of predominantly hydrophobic poly(styrene)-poly(ethylene oxide) copolymers at air/water and cyclohexane/water interfaces. *Langmuir* 1999, 15, 6127–6131.
- (42) Paturej, J.; Sheiko, S. S.; Panyukov, S.; Rubinstein, M. Molecular structure of bottlebrush polymers in melts. *Sci. Adv.* **2016**, 2, No. e1601478.
- (43) Hokajo, T.; Terao, K.; Nakamura, Y.; Norisuye, T. Solution Properties of Polymacromonomers Consisting of Polystyrene v. Effect of Side Chain Length on Chain Stiffness. *Polym. J.* **2001**, 33, 481–485.
- (44) Gauge, A.; Pakula, T. Static Properties of Noninteracting Comb Polymers in Dense and Dilute Media. A Monte Carlo Study. *Macromolecules* **1995**, 28, 190–196.
- (45) Wintermantel, M.; Gerle, M.; Fischer, K.; Schmidt, M.; Wataoka, I.; Urakawa, H.; Kajiwara, K.; Tsukahara, Y. Molecular bottlebrushes. *Macromolecules* **1996**, 29, 978–983.
- (46) Liu, X.; Thormann, E.; Dedinaite, A.; Rutland, M.; Visnevskij, C.; Makuska, R.; Claesson, P. M. Low friction and high load bearing capacity layers formed by cationic-block-non-ionic bottle-brush copolymers in aqueous media. *Soft Matter* **2013**, *9*, 5361–5371.
- (47) Willets, K. A.; Van Duyne, R. P. Localized surface plasmon resonance spectroscopy and sensing. *Annu. Rev. Phys. Chem.* **2007**, *58*, 267–297.
- (48) Dunn, O. J. Multiple Comparisons Using Rank Sums. *Technometrics* **1964**, *6*, 241–252.
- (49) Oron, A. P. H.; Peter, D. Kruskal-Wallis and Friedman Type Tests for Nested Effects in Hierarchical Designs; University of Washington, 2006.
- (50) Navarro, L. A.; French, D. L.; Zauscher, S. Synthesis of Modular Brush Polymer-Protein Hybrids Using Diazotransfer and Copper Click Chemistry. *Bioconjugate Chem.* **2018**, *29*, 2594–2605.
- (51) Katz, B. A.; Cass, R. T. In crystals of complexes of streptavidin with peptide ligands containing the HPQ sequence the pKa of the peptide histidine is less than 3.0. *J. Biol. Chem.* **1997**, 272, 13220–13228.
- (52) Majorek, K. A.; Porebski, P. J.; Dayal, A.; Zimmerman, M. D.; Jablonska, K.; Stewart, A. J.; Chruszcz, M.; Minor, W. Structural and immunologic characterization of bovine, horse, and rabbit serum albumins. *Mol. Immunol.* **2012**, *52*, 174–182.
- (53) Magalhães, M. L. B.; Czekster, C. M.; Guan, R.; Malashkevich, V. N.; Almo, S. C.; Levy, M. Evolved streptavidin mutants reveal key role of loop residue in high-affinity binding. *Protein Sci.* **2011**, *20*, 1145–1154.
- (54) Lutz, J.-F. Polymerization of oligo(ethylene glycol) (meth)-acrylates: Toward new generations of smart biocompatible materials. *J. Polym. Sci., Part A: Polym. Chem.* **2008**, *46*, 3459–3470.
- (55) Nilebäck, E.; Feuz, L.; Uddenberg, H.; Valiokas, R.; Svedhem, S. Characterization and application of a surface modification designed for QCM-D studies of biotinylated biomolecules. *Biosens. Bioelectron.* **2011**, 28, 407–413.
- (56) Barth, A. Infrared spectroscopy of proteins. *Biochim. Biophys. Acta* **2007**, *1767*, 1073–1101.
- (57) Bandey, H. L.; Martin, S. J.; Cernosek, R. W.; Hillman, A. R. Modeling the Responses of Thickness-Shear Mode Resonators under Various Loading Conditions. *Anal. Chem.* 1999, 71, 2205–2214.
- (58) Ge, T.; Rubinstein, M. Strong Selective Adsorption of Polymers. *Macromolecules* **2015**, 48, 3788–3801.
- (59) Singh, N.; Karim, A.; Bates, F. S.; Tirrell, M.; Furusawa, K. Adsorption of End-Functionalized Polystyrene on Model Textured Surfaces. *Macromolecules* **1994**, *27*, 2586–2594.
- (60) Luzinov, I.; Julthongpiput, D.; Malz, H.; Pionteck, J.; Tsukruk, V. V. Polystyrene layers grafted to epoxy-modified silicon surfaces. *Macromolecules* **2000**, *33*, 1043–1048.

- (61) Rathgeber, S.; Pakula, T.; Wilk, A.; Matyjaszewski, K.; Beers, K. L. On the shape of bottle-brush macromolecules: systematic variation of architectural parameters. *J. Chem. Phys.* **2005**, *122*, 124904.
- (62) Zhulina, Y. B.; Pryamitsyn, V. A.; Borisov, O. V. Structure and Conformational Transitions in Grafted Polymer Chain Layers. A New Theory. *Polym. Sci.* **1989**, *31*, 205–216.
- (63) Szleifer, I.; Carignano, M. A. Tethered Polymer Layers; Wiley: New York, 1996; Vol. 94.
- (64) Zhang, G.; Wu, C. Quartz Crystal Microbalance Studies on Conformational Change of Polymer Chains at Interface. *Macromol. Rapid Commun.* **2009**, *30*, 328–335.
- (65) Ou-Yang, H. D.; Gao, Z. A Pancake-to-Brush Transition in Polymer Adsorption. J. Phys. II 1991, 1, 1375–1385.
- (66) Xiong, W.; Qiu, X.; Zhong, R.; Yang, D. Characterization of the adsorption properties of a phosphorylated kraft lignin-based polymer at the solid/liquid interface by the QCM-D approach. *Holzforschung* **2016**, 70, 937–945.
- (67) Plunkett, M. A.; Wang, Z.; Rutland, M. W.; Johannsmann, D. Adsorption of pNIPAM layers on hydrophobic gold surfaces, measured in situ by OCM and SPR. *Langmuir* **2003**, *19*, 6837–6844.
- (68) Ma, H.; Textor, M.; Clark, R. L.; Chilkoti, A. Monitoring kinetics of surface initiated atom transfer radical polymerization by quartz crystal microbalance with dissipation. *Biointerphases* **2006**, *1*, 35–39.
- (69) Navarro, L. A.; Enciso, A. E.; Matyjaszewski, K.; Zauscher, S. Enzymatically Degassed Surface-Initiated Atom Transfer Radical Polymerization with Real-Time Monitoring. *J. Am. Chem. Soc.* **2019**, 141, 3100–3109.
- (70) Huang, H.; Cammers, A.; Penn, L. S. Grafting of free chains in the presence of preexisting polymer brushes. *Macromolecules* **2006**, 39, 7064–7070.
- (71) Yuan, C.; Chen, A.; Kolb, P.; Moy, V. T. Energy landscape of streptavidin-biotin complexes measured by atomic force microscopy. *Biochemistry* **2000**, *39*, 10219–10223.
- (72) Jay, G. D.; Tantravahi, U.; Britt, D. E.; Barrach, H. J.; Cha, C.-J. Homology of lubricin and superficial zone protein (SZP): products of megakaryocyte stimulating factor (MSF) gene expression by human synovial fibroblasts and articular chondrocytes localized to chromosome 1q25. *J. Orthop. Res.* **2001**, *19*, 677–687.
- (73) Swann, D. A.; Slayter, H. S.; Silver, F. H. The molecular structure of lubricating glycoprotein-I, the boundary lubricant for articular cartilage. *J. Biol. Chem.* 1981, 256, 5921.
- (74) Estrella, R. P.; Whitelock, J. M.; Packer, N. H.; Karlsson, N. G. The glycosylation of human synovial lubricin: implications for its role in inflammation. *Biochem. J.* **2010**, 429, 359–367.